Chemical Science

ROYAL SOCIETY OF CHEMISTRY

EDGE ARTICLE

View Article Online
View Journal | View Issue

Cite this: *Chem. Sci.*, 2025, **16**, 16659

All publication charges for this article have been paid for by the Royal Society of Chemistry

Received 6th May 2025
Accepted 6th August 2025

DOI: 10.1039/d5sc03295d

rsc.li/chemical-science

$BiVO_4$/BiOCl heterostructure photoanodes for highly selective photoelectrochemical oxidation of benzylic C(sp^3)–H bonds

Haiwen Shi,[a] Qingjie Wang,[a] Youai Qiu [bcd] and Jingshan Luo *[acd]

Photoelectrochemical (PEC) activation of benzylic C(sp^3)–H bonds offers a sustainable and eco-friendly approach to synthesizing high-value chemicals. However, achieving high selectivity for desired products remains a significant challenge. In this study, we developed a BiOCl-modified $BiVO_4$ ($BiVO_4$/BiOCl) heterostructure photoanode for the PEC oxidation of benzylic C(sp^3)–H bonds. The p–n heterojunction formed between BiOCl and $BiVO_4$ enhances charge carrier separation and transport, while the BiOCl surface layer facilitates the desorption of benzaldehyde. As a result, the optimized $BiVO_4$/BiOCl photoanode demonstrated nearly 100% selectivity for benzaldehyde production and had similar applicability to a range of benzylic C(sp^3)–H bond compounds. The reaction mechanism was further elucidated through *in situ* FTIR spectroscopy. Additionally, a scalable flow cell integrating the $BiVO_4$/BiOCl photoanode with a Pt/C-GDE achieved a 77% selectivity in continuous toluene-to-benzaldehyde conversion, and the ability to activate the C(sp^3)–H bonds using sunlight without bias was demonstrated. This work highlights a promising strategy for solar-driven organic synthesis, advancing the integration of renewable energy into chemical manufacturing.

Introduction

The activation of benzylic C(sp^3)–H bonds is pivotal in organic chemistry due to their widespread presence in organic molecules and their potential for synthesizing high-value chemicals.[1–8] For example, benzaldehyde, which is widely used in the preparation of pharmaceuticals and other chemicals, is produced from toluene, one of the most representative C(sp^3)–H bond alkyl aromatic hydrocarbons. However, its industrial production strategies nowadays rely on toluene chlorination or liquid-phase oxidation at high temperature and high pressure due to the nonpolar nature and high C(sp^3)–H bond energy.[9] Meanwhile, those strategies suffer from large amounts of peroxide byproducts and toxic waste.[10,11] Considering that the global gross annual demand of benzaldehyde in 2022 has reached over 170 kt, and this value is expected to reach approximately 240 kt by 2032, there is an urgent need for a more environmentally friendly approach for benzaldehyde production.[12]

The photoelectrochemical (PEC) approach has been widely studied for converting solar energy into hydrogen through water splitting.[13–19] Under illumination, the photogenerated charge carriers can provide effective oxidation and reduction capabilities, making the PEC approach promising for green organic synthesis under mild conditions.[20–25] Previous studies have demonstrated the feasibility of this approach, such as the construction of C–N and C–P bonds,[26–28] the generation of trifluoromethyl compounds,[29] the oxidation of glycerol,[30,31] and the epoxidation reaction.[32–34] Recently, Yang *et al.*[35] used ·OH generated by oxygen reduction on the $CuBi_2O_4$ photocathode to activate toluene indirectly to produce benzaldehyde. However, considering that the efficiency or selectivity of this indirect activation strategy may be limited by the generation of ·OH, direct activation of benzylic C(sp^3)–H bonds using photogenerated holes is more promising for achieving efficient benzaldehyde synthesis. There are studies on the selective generation of benzaldehyde *via* photochemical (PC)[36–44] and electrochemical (EC)[11,45–47] approaches using toluene directly as a substrate. Considering that the PEC approach has the advantages of separation of cathode and anode reactions and is directly driven by sunlight, the study of the PEC toluene oxidation is of great significance for promoting the application of sustainable and more complex cascade organic synthesis in the future.[48–50]

[a]*Institute of Photoelectronic Thin Film Devices and Technology, State Key Laboratory of Photovoltaic Materials and Cells, Tianjin Key Laboratory of Efficient Solar Energy Utilization, Ministry of Education Engineering Research Center of Thin Film Photoelectronic Technology, Nankai University, Tianjin 300350, China. E-mail: jingshan.luo@nankai.edu.cn*

[b]*State Key Laboratory of Elemento-Organic Chemistry, College of Chemistry, Nankai University, Tianjin 300071, China*

[c]*Frontiers Science Center for New Organic Matter, Nankai University, Tianjin 300071, China*

[d]*Academy for Advanced Interdisciplinary Studies, Nankai University, Tianjin 300071, China*

In this work, we developed a heterostructure $BiVO_4$/BiOCl photoanode for converting toluene into benzaldehyde, achieving both a high toluene conversion rate and a high benzaldehyde selectivity. BiOCl nanosheets formed a heterojunction structure with $BiVO_4$, enhancing the charge separation efficiency, and promoting the activation of benzylic C(sp^3)–H bonds of toluene by photogenerated holes and $\cdot O_2^-$ generation by photogenerated electrons on the counter electrode. Meanwhile, BiOCl avoided the adsorption of benzaldehyde on the photoanode, thus maintaining a high benzaldehyde selectivity. As a result, with additional O_2 as the oxygen resource, this heterostructure photoanode achieved a toluene conversion rate of nearly 40% and a benzaldehyde selectivity of 98.9% with a yield rate of 9.64 μmol cm^{-1} h^{-1}. Meanwhile, this photoanode exhibited a broad substrate scope for the oxidation of benzylic C(sp^3)–H bonds. Furthermore, we identified a safer and more economical condition by utilizing atmospheric oxygen, achieving over 30% toluene conversion while maintaining nearly 100% benzaldehyde selectivity. In addition, we built a scalable flow cell to realize the high-selectivity synthesis of benzaldehyde and demonstrated its potential for benzaldehyde production under bias-free conditions using only sunlight.

Results and discussion

Photoanode preparation and characterization

The $BiVO_4$ photoanode was prepared using a previously reported method with slight modification,[51] whereas BiOCl was grown using electrodeposition, followed by annealing and an acid-mediated chemical reaction.[52,53] The details are available in the SI. X-ray diffraction (XRD) patterns of $BiVO_4$ and $BiVO_4$/BiOCl thin films are shown in Fig. 1a, confirming that the prepared photoanodes matched the monoclinic $BiVO_4$ structure. Notably, the $BiVO_4$/BiOCl photoanode showed the diffraction peaks of BiOCl, indicating the successful construction of the $BiVO_4$/BiOCl heterojunction. Meanwhile, the XRD pattern of the BiOCl/FTO electrode also matched the standard PDF pattern (Fig. S1). BiOCl is a large bandgap p-type semiconductor that crystallizes in a tetragonal structure. The ultraviolet-visible (UV-vis) absorption spectra of $BiVO_4$ and BiOCl thin films revealed adsorption onset values *ca.* 500 nm and 380 nm (Fig. S2), respectively, consistent with the reported band gaps of 2.54 and 3.56 eV (Fig. S3). Scanning electron microscope (SEM) images reveal that the prepared $BiVO_4$ photoanode exhibited a porous worm-like morphology (Fig. S4), while BiOCl deposition increased the surface roughness and displayed an ultra-thin nanosheet-modified $BiVO_4$ surface (Fig. 1b), which was further confirmed using the SEM image of the BiOCl/FTO electrode (Fig. S5). Additionally, energy-dispersive X-ray (EDX) spectroscopy revealed the uniform distribution of the Cl element aligned with these flower-like structures (Fig. S6 and S7). Transmission electron microscopy (TEM) and high-resolution transmission electron microscopy (HRTEM) images confirm that the prepared $BiVO_4$ had a well-defined crystal structure, with a lattice spacing of 0.24 nm corresponding to the monoclinic $BiVO_4$ (202) crystal plane (Fig. S8). The spherical aberration-corrected transmission electron microscope (AC-TEM) image of the $BiVO_4$/BiOCl photoanode showed a 0.134 nm lattice spacing, corresponding to the (204) crystal plane of BiOCl (Fig. 1c). The TEM image (Fig. 1d) and EDX results (Fig. 1e–h) further demonstrated a nanosheet-like morphology of BiOCl. Notably, the larger coverage area of Cl compared to V further illustrated that BiOCl was coated on $BiVO_4$. The chemical composition and elemental states of the $BiVO_4$ and $BiVO_4$/BiOCl photoanodes were determined by X-ray photoelectron spectroscopy (XPS). As shown in Fig. 1i and j, the difference in binding energy between the two signal peaks of Bi 4f was 5.3 eV, and that of V 2p was 7.6 eV, proving that Bi and V existed in the form of Bi^{3+} and V^{5+}, respectively. In addition, the Bi 4f and V 2p spectra exhibited a slight shift toward higher binding energies for $BiVO_4$/BiOCl, suggesting the interaction between BiOCl and $BiVO_4$.[54] Furthermore, the Cl 2p signal was also detected in the $BiVO_4$/BiOCl photoanode (Fig. 1k), confirming the successful fabrication of the $BiVO_4$/BiOCl heterojunction.

Evaluation of photoanode performance

The PEC cell with a three-electrode configuration comprising a photoanode, counter electrode (Pt), and reference electrode (Ag/AgCl) was often used for studying the conversion of solar energy into chemical fuels (Fig. 2a). Typically, the evolution of oxygen and hydrogen occurs at the photoanode and counter electrode in an aqueous electrolyte, respectively. In this work, instead of using an aqueous electrolyte, the organic synthesis system utilized the organic electrolyte MeCN containing the reactant substrate toluene. The toluene is oxidized at the photoanode, subsequently undergoing a series of chemical reactions to form the desired target product, benzaldehyde (Fig. 2b). The PEC response of both $BiVO_4$/BiOCl and $BiVO_4$ photoanodes was recorded in a single-chamber PEC cell with a three-electrode configuration under simulated (AM 1.5G) solar illumination (Fig. S12).

As shown in Fig. S14, the photocurrent density recorded at 0.65 V *vs.* Fc/Fc^+ increased from 0.4 mA cm^{-2} ($BiVO_4$) to 0.6 mA cm^{-2} ($BiVO_4$/BiOCl) in the presence of toluene, accompanied by a cathodic shift of the onset potential from 0.4 to 0.3 V *vs.* Fc/Fc^+, indicating that the fabricated $BiVO_4$/BiOCl heterojunction increased charge separation efficiency. In addition, both photoanodes exhibited higher activity in the presence of toluene compared to the electrolyte without toluene, revealing that toluene can be efficiently oxidized in this PEC system. Furthermore, Fig. 2c shows that the oxygen-rich environment was beneficial for toluene oxidation, and the photocurrent density of $BiVO_4$/BiOCl reached 0.7 mA cm^{-2} in the presence of O_2 at 0.65 V *vs.* Fc/Fc^+, indicating that the oxidation of toluene might be related to the activation of O_2, in agreement with the previous report that O_2 provided the oxygen source and accelerated the formation of benzaldehyde.[36–39] To elucidate the impact of surface treatment on the charge transport properties, electrochemical impedance spectroscopy (EIS) of both $BiVO_4$ and $BiVO_4$/BiOCl photoanodes was performed and the results are displayed in Fig. S15. Notably, the $BiVO_4$/BiOCl photoanode demonstrated a smaller semicircle than $BiVO_4$ in the toluene/

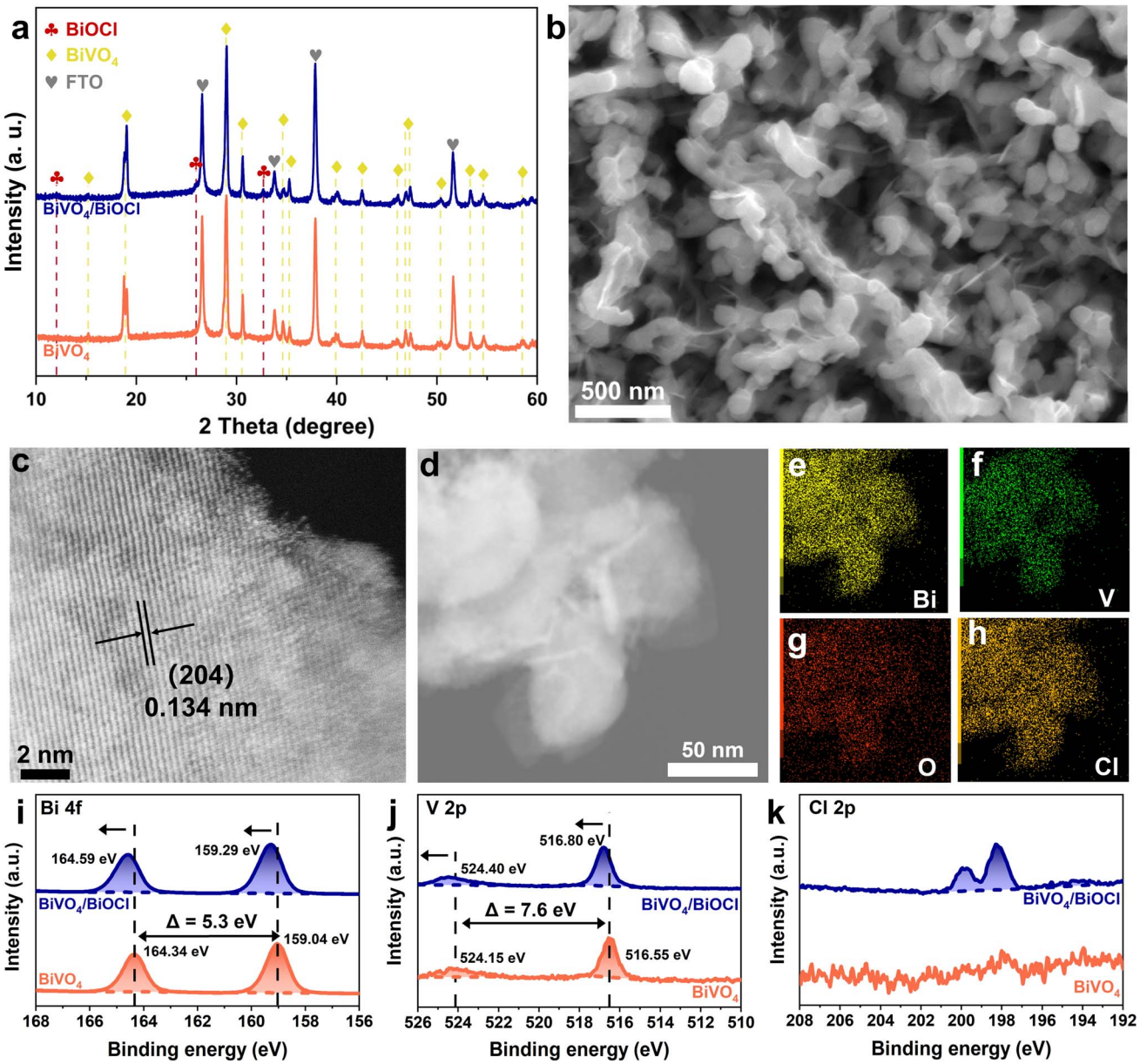

Fig. 1 (a) XRD spectra of $BiVO_4$ and $BiVO_4$/BiOCl. (b) SEM image of $BiVO_4$/BiOCl. (c) AC-TEM image of $BiVO_4$/BiOCl. (d) TEM image and (e–h) corresponding EDX mapping images of $BiVO_4$/BiOCl. (i) XPS Bi 4f spectra, (j) XPS V 2p spectra, and (k) XPS Cl 2p spectra of $BiVO_4$ and $BiVO_4$/BiOCl.

MeCN system, indicating that the formed heterojunction promoted charge separation. Moreover, Mott–Schottky (M–S) plots measured in the aqueous solution were used to analyze $BiVO_4$ and BiOCl thin films. Notably, $BiVO_4$ and BiOCl exhibited typical positive and negative slopes in the entire potential range, in agreement with the n-type and p-type semiconductor properties, respectively. The flat band potential of $BiVO_4$ and BiOCl is *ca.* 0.29 V_{NHE} and 2.40 V_{NHE}, respectively (Fig. S16). In general, the flat band potential is approximately equal to the Fermi level. Based on the above results, the schematic energy band structure of $BiVO_4$ and BiOCl exhibits a typical p–n heterojunction (Fig. S17), which is anticipated to effectively promote charge separation.

The toluene oxidation performance was evaluated at 0.65 V *vs.* Fc/Fc^+ for 4 h under AM 1.5G illumination in a single-chamber PEC cell. The $BiVO_4$/BiOCl photoanode showed a higher toluene conversion ability than $BiVO_4$ in the presence of O_2, accompanied by the benzaldehyde selectivity (based on the amount of toluene converted) of $BiVO_4$/BiOCl and $BiVO_4$ reaching 98.9% and 66.6%, respectively, indicating that BiOCl can promote the toluene conversion and the benzaldehyde selectivity (Fig. 2d). More importantly, the Faraday efficiency (FE) of the $BiVO_4$/BiOCl photoanode reached approximately 96% for benzaldehyde production, which was much higher than 76% of the $BiVO_4$ photoanode (Fig. 2e). In the Ar environment, there was no benzaldehyde generated for the $BiVO_4$

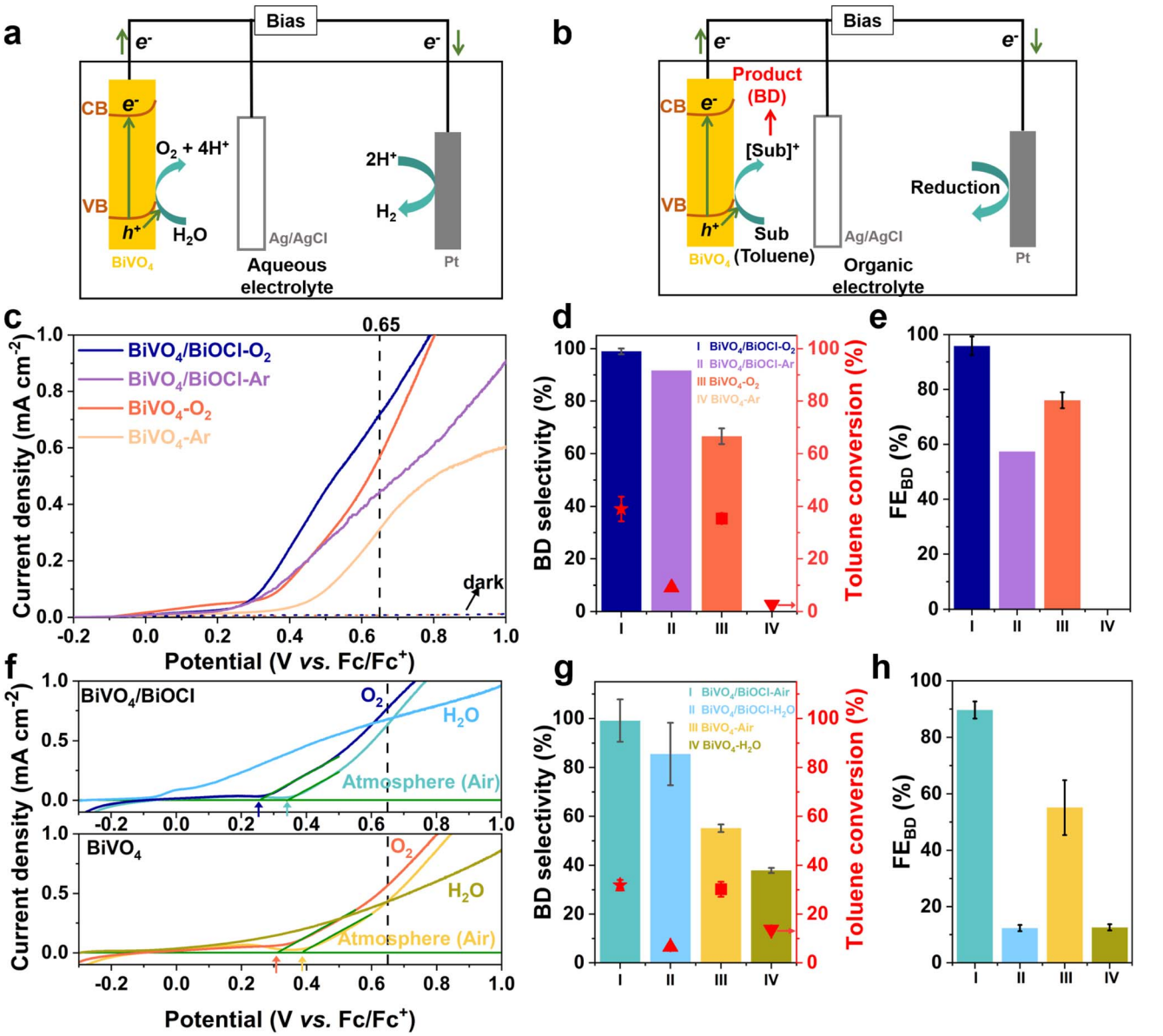

Fig. 2 (a) The schematic diagram of a PEC water splitting system. (b) The schematic diagram of a PEC organic synthesis system. (c) LSV curves, (d) toluene conversion rate, benzaldehyde selectivity, and (e) FE for $BiVO_4$/BiOCl and $BiVO_4$ with O_2 or Ar purged in. (f) LSV curves, (g) toluene conversion rate, benzaldehyde selectivity, and (h) FE for $BiVO_4$/BiOCl and $BiVO_4$ in the atmosphere or MeCN containing 5% H_2O. Reaction potential, 0.65 V *vs.* Fc/Fc$^+$. Reaction time, 4 h. Electrolyte, 0.1 M $LiClO_4$/MeCN. Substrate, 10 mM toluene. BD represents benzaldehyde.

photoanode, indicating that O_2 was necessary for the formation of benzaldehyde. The residual H_2O from the electrolyte (Fig. S18) might participate in the reaction since the $BiVO_4$/BiOCl photoanode still achieved over 90% selectivity for benzaldehyde. Therefore, BiOCl and activated oxygen work together to achieve nearly 100% benzaldehyde selectivity.

The above results have confirmed that O_2 played an indispensable role in the oxidation of toluene to benzaldehyde. However, considering the high cost of high-purity O_2, using atmospheric O_2 or H_2O as an alternative oxygen source is a more promising strategy. As shown in Fig. 2f, reactions conducted with the feed of air showed a lower current density and a later onset potential for both photoanodes, indicating that a higher concentration of O_2 promoted the conversion of toluene. Although the toluene conversion on both photoanodes under atmospheric conditions was reduced compared to that with additional O_2 purged in, the $BiVO_4$/BiOCl photoanode still exhibited excellent performance in benzaldehyde production, with the selectivity and FE of benzaldehyde reaching about 100% and 90%, respectively (Fig. 2g and h). In the presence of MeCN containing 5% H_2O, both $BiVO_4$/BiOCl and $BiVO_4$ photoanodes showed a lower onset potential, while the photocurrent remained unchanged compared to that in the atmosphere, indicating that H_2O splitting might compete with toluene oxidation. In addition, the selectivity of benzaldehyde of $BiVO_4$/BiOCl and $BiVO_4$ decreased to 85.5% and 37.9%, respectively,

indicating the competitive reaction of water oxidation in this case. Correspondingly, the benzaldehyde FE of $BiVO_4$/BiOCl decreased to 12.4%, indicating that a large number of photogenerated holes are involved in the water oxidation reaction. It should be noted that the amount of H_2O added to the MeCN/H_2O electrolyte was over 150 times the amount of residual H_2O in the pure MeCN electrolyte. The residual H_2O in the pure MeCN electrolyte was not enough to cause a competitive reaction with toluene oxidation. These results demonstrate that this PEC system can achieve efficient benzaldehyde generation under atmospheric conditions without the need for pure O_2 feed.

To demonstrate the broad applicability of the PEC strategy for benzylic C(sp^3)–H bond activation using the $BiVO_4$/BiOCl photoanode, a wide range of substrates bearing electron-rich and electron-deficient substituents were evaluated. These included methyl (1–3), methyl formate (4), halogens (5–7), and cyanide (8), all of which were efficiently oxygenated to their corresponding aldehydes (Fig. 3). Notably, the *ortho*-methyl-substituted substrate exhibited high selectivity, while the *meta*- and *para*-methyl-substituted toluenes showed higher conversion rates but lower selectivity, attributed to the formation of isophthalaldehyde and terephthalaldehyde (Fig. S22b and c). Additionally, *para*-substituted toluenes with various electron-withdrawing groups (4–8) also underwent efficient oxygenation with excellent selectivity, indicating good compatibility with diverse functional groups.

We also explored the oxidation of benzylic C(sp^3)–H bonds to form ketones. Both ethylbenzene (9) and diphenylmethane (10) showed high selectivity toward their respective ketones. However, oxidation of 1,2,3,4-tetrahydronaphthalene (11) resulted in lower selectivity, likely due to dehydrogenation to form naphthalene (Fig. S22k). Collectively, these results further underscore the strong PEC activity of the $BiVO_4$/BiOCl photoanode and its broad substrate compatibility.

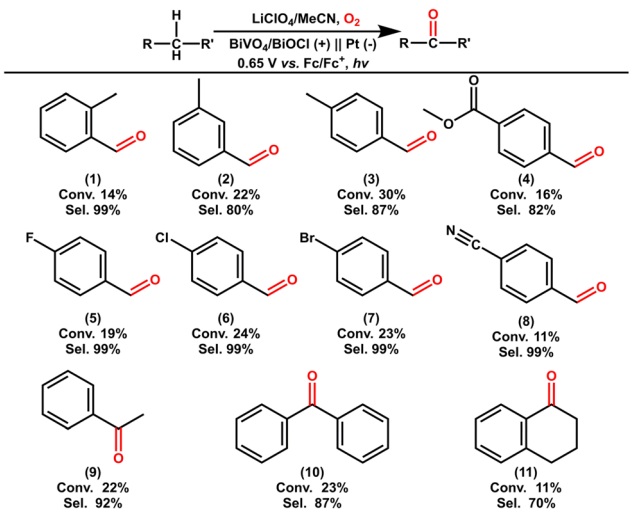

Fig. 3 Selective oxidation of various C(sp^3)–H derivatives on the $BiVO_4$/BiOCl photoanode with O_2 purged in. Reaction potential, 0.65 V *vs.* Fc/Fc^+. Reaction time, 4 h (entries 1–3, 5–7, and 9–11) and 8 h (entries 4 and 8). Electrolyte, 0.1 M $LiClO_4$/MeCN. Substrate, 10 mM C(sp^3)–H derivative.

Reaction mechanism of toluene oxidation in the PEC system

To understand the reaction mechanism of PEC toluene oxidation, a series of quenching experiments were conducted to find out the main active species (Fig. 4a). After tetra-methylpiperidine *N*-oxide (TEMPO) was added to quench all radicals, the conversion rate of toluene and concentration of benzaldehyde were suppressed to less than 5% and 0.5 mM, respectively, indicating that this reaction is a radical reaction. Butylated hydroxytoluene (BHT) and $NH_4C_2O_4$ were added to capture benzyl radicals and photogenerated holes, respectively. Both groups limited the benzaldehyde concentration to approximately 1.2 mM with a toluene conversion rate lower than 15%, demonstrating that benzyl radicals and holes participated in the reaction. The addition of benzoquinone (BQ) as an $\cdot O_2^-$ scavenger restrained the generation of benzaldehyde, suggesting that $\cdot O_2^-$ is one of the important species. The results of these experiments reveal to us that photogenerated holes, benzyl radicals, and $\cdot O_2^-$ play a role in this reaction.

Fig. 4b and c show the toluene conversion and benzaldehyde selectivity curves over time for the two kinds of photoanodes. Both exhibited similar toluene conversion properties, but the selectivity of benzaldehyde displayed different results. To understand the reason that the $BiVO_4$/BiOCl photoanode displayed a higher photocurrent but exhibited a limited toluene conversion gain compared with $BiVO_4$, a kinetic isotope effect (KIE) experiment was used to find out the rate-determining step (RDS), and the final result shows that the C(sp^3)–H bond activation was the RDS since the k_H/k_D value was around 2 during the whole test (Fig. S23).[55–57] Meanwhile, the former research showed that the electrolyte contained impurity H_2O, indicating that while the heterojunction structure allowed the photoanode to exhibit a higher photocurrent, the enhanced photocurrent may not only originate from the reaction between photogenerated holes and C(sp^3)–H bonds but also potentially from the reaction with residual H_2O from the electrolyte, thus resulting in a limited conversion rate. These results also explain the reason why PEC systems using $BiVO_4$/BiOCl as the photoanode achieved nearly 100% benzaldehyde selectivity, but FE cannot reach the same high value. As for the benzaldehyde selectivity, the $BiVO_4$ photoanode exhibited a high benzaldehyde selectivity in the first hour, but it began to decrease as the reaction continued, while the modified photoanode maintained a high selectivity during the whole reaction. As shown in GC spectra (Fig. S24), the generation of benzyl ether can be a reason for the loss of selectivity, which was formed by the benzyl radical. The PEC toluene oxidation conducted in the two-chamber H-cell confirmed that $\cdot O_2^-$ was formed on the counter electrode by the reduction of O_2 since there was almost no benzaldehyde generated in the anode chamber (Fig. 4d), also further indicating that the formation of benzaldehyde is influenced by the generation of $\cdot O_2^-$. Compared to the modified heterojunction photoanode, due to the poor carrier separation efficiency of $BiVO_4$, the reaction rate of toluene and $\cdot O_2^-$ formation was

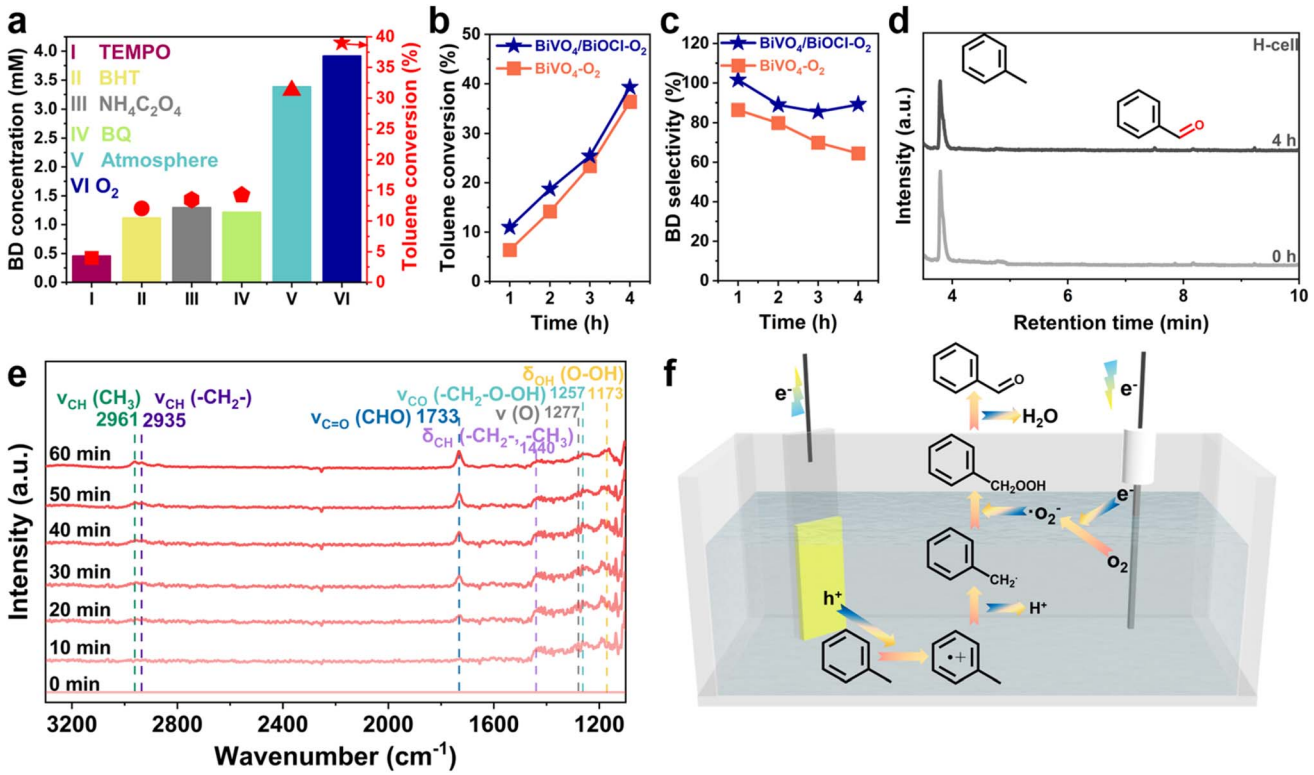

Fig. 4 (a) Quenching experiments of toluene oxidation. (b) Evolution of toluene conversion and (c) benzaldehyde selectivity as a function of reaction time for $BiVO_4$ and $BiVO_4$/BiOCl with O_2 purged in. (d) GC spectra from the solution in the anode chamber of the H-cell using $BiVO_4$/BiOCl as the photoanode. (e) *In situ* DRIFTS of toluene oxidation using $BiVO_4$/BiOCl as the photoanode. (f) Proposed mechanism for toluene oxidation over the $BiVO_4$/BiOCl photoanode. BD represents benzaldehyde.

limited, resulting in the recombination of benzyl radicals to form benzyl ether.

To further reveal the reaction pathway, the *in situ* Fourier transform infrared (FTIR) spectra test was conducted on the $BiVO_4$/BiOCl photoanode. As shown in Fig. 4e, with the gradual increase in reaction time, a signal peak attributed to the carbon–oxygen double bond of the aldehyde group appeared at 1733 cm^{-1}, and the peak area increased with time, proving the generation of benzaldehyde.[58,59] Meanwhile, a methylene signal peak appeared at 2935 cm^{-1}, and the peak intensity also increased with time, indicating that the C(sp^3)–H bonds of toluene were oxidized by photogenerated holes.[38] In addition, weak signal peaks at 1173 and 1257 cm^{-1} attributed to hydroperoxide species were gradually detected as the reaction progressed,[37,38] suggesting that hydroperoxide species may be intermediates in the reaction process. The *in situ* FTIR test using the $BiVO_4$ photoanode was also conducted to understand the difference between the two photoanodes during the reaction (Fig. S25). Peaks belonging to the aldehyde group red-shifted to around 1728 cm^{-1}, indicating that the $BiVO_4$ photoanode has a stronger adsorption capacity for benzaldehyde compared to the modified photoanode.[38] This stronger adsorption led to the overoxidation of benzaldehyde and a decrease in selectivity, as evidenced by the appearance of CO_2 signal peaks (2337 and 2362 cm^{-1}) after 40 minutes, while there were no CO_2 peaks for the $BiVO_4$/BiOCl photoanode.[60–62] At 1275 cm^{-1}, a signal peak attributed to the adsorbed oxygen species showed a different trend compared to the results observed with the modified photoanode.[39] On the $BiVO_4$/BiOCl photoanode, the intensity of the adsorbed oxygen species signal was much weaker than that measured on the $BiVO_4$ photoanode, and it decreased gradually as the reaction proceeded, indicating the occurrence of oxygen transfer during the reaction. However, on the $BiVO_4$ photoanode, the stronger signal intensity and its further enhancement over time suggest that the oxygen transfer process was inhibited. Additionally, the mixed peaks of methyl and methylene at around 1440 cm^{-1} in both spectra show similar distinctions, suggesting that the poor carrier separation and transfer efficiency of the $BiVO_4$ photoanode limited benzaldehyde production.

Based on these experimental results, the reaction mechanism and pathway of this PEC toluene oxidation reaction can be explained as follows (Fig. 4f). First, toluene is absorbed on the photoanode and transferred to the toluene molecular cation by photogenerated holes, which then loses H^+ to form the benzyl radical.[38,63,64] Meanwhile, due to the heterojunction structure formed between BiOCl and $BiVO_4$, the separation of photogenerated electron–hole pairs is accelerated, facilitating the transfer of photogenerated electrons to the counter electrode, reducing O_2 to $\cdot O_2^-$. The benzyl radical and $\cdot O_2^-$ then react with each other to form the hydroperoxide species. Finally, the hydroperoxide species can be dehydrated to produce

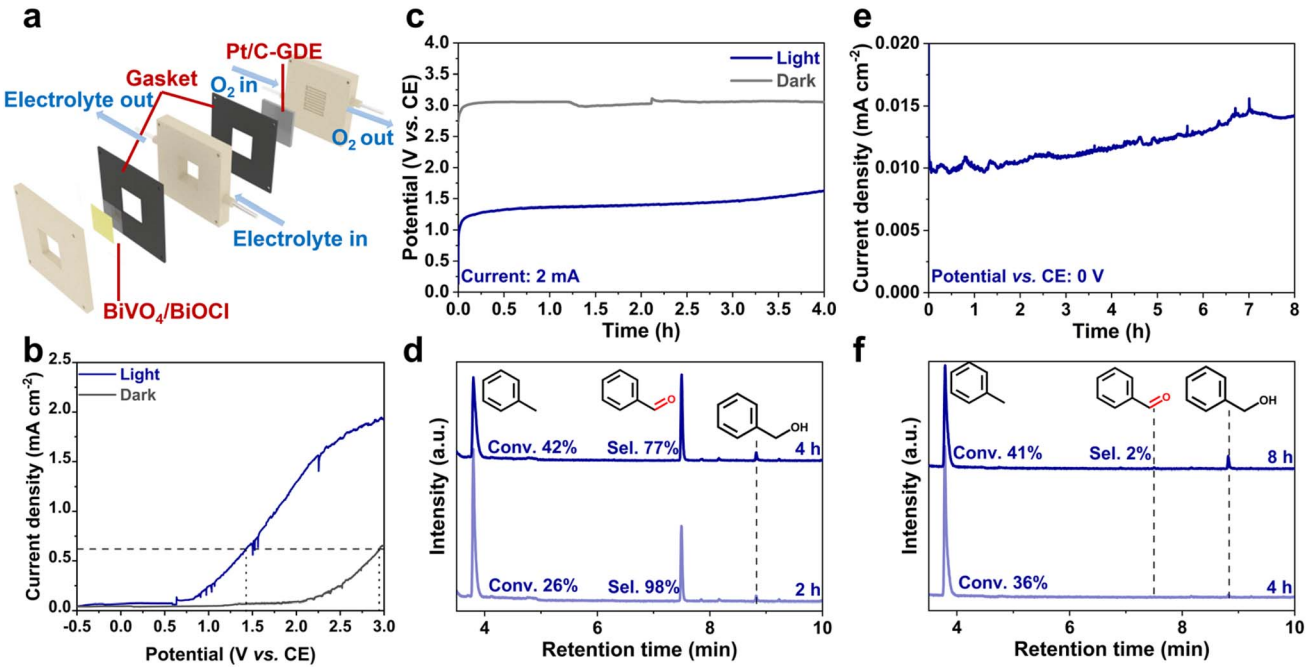

Fig. 5 (a) The layout of the homemade flow cell. (b) LSV curves of the scale-up $BiVO_4$/BiOCl photoanode in the flow cell. (c) Evolution of the cell potential as a function of time during constant current reaction. (d) GC spectra of the flow cell in a constant current reaction mode with illumination. (e) *J*–*t* curve of the bias-free flow cell without bias. (f) GC spectra of the bias-free flow cell. BD represents benzaldehyde.

benzaldehyde, and the benzaldehyde desorbs from the photoanode to avoid overoxidation. It should be noted that H_2O formed by the dehydration of the intermediate was only 0.72 μL at the highest conversion rate and selectivity, and the possibility of its competing reaction with toluene oxidation can be completely ignored.

PEC toluene oxidation demonstration in a flow cell

Since we have realized the production of benzaldehyde *via* PEC toluene oxidation, we further attempted to conduct this reaction continuously in a homemade scale-up flow cell. This flow cell consists of two chambers to ensure gas tightness, one serving as a reaction chamber for the flow of the electrolyte and the other as a gas channel chamber for the flow of O_2, separated by a gas diffusion electrode loaded with Pt/C (Pt/C-GDE) serving as the counter electrode (Fig. 5a).

The reaction in the flow cell was conducted in a constant current mode under 2 mA, and this current density is approximately the same as the current density in the single chamber cell since 1.8 × 1.8 cm^2 $BiVO_4$/BiOCl was used as the photoanode. During the constant current reaction, the cell voltage was about 3 V in the dark, while the photoanode can reduce the demand for external voltage to 1.4 V under illumination, both matching LSV results (Fig. 5b and c). In the first 2 hours, this flow cell can reach a 98% selectivity of benzaldehyde with 26% conversion of toluene. However, after the 4-hour reaction, the selectivity of benzaldehyde decreased to 77% (Fig. 5d). Compared to the GC results in our former experiments, the GC spectra displayed the signal peak of benzyl alcohol. According to the research of Xue *et al.*,[38] there is another pathway to convert toluene to benzaldehyde. The toluene is first converted to the benzyl radical, and then the benzyl radical directly reacts with O_2 to generate benzyl alcohol, which is further oxidized to benzaldehyde by photogenerated holes. Therefore, the decrease in benzaldehyde selectivity can be attributed to the poorer O_2 reduction performance of the Pt/C-GDE compared to the conventional Pt electrode, which failed to effectively reduce O_2 to $\cdot O_2^-$, leading to the direct combination of O_2 and the benzyl radical to form benzyl alcohol. Moreover, as the reaction time extended, the performance of the Pt/C-GDE deteriorated further, exacerbating this phenomenon.

Besides, a bias-free toluene oxidation reaction was tried in this flow cell. Fig. 5e shows that the $BiVO_4$/BiOCl photoanode can provide about 0.01–0.015 mA cm^{-2} photocurrent density during the 8-hour bias-free reaction. During the first 4 hours, there was only benzyl alcohol generated according to the GC spectra, and with the gradual extension of the reaction time, a trace amount of benzaldehyde was eventually obtained, with a selectivity of approximately 2% (Fig. 5f). This result demonstrates the feasibility of PEC toluene oxidation under unbiased conditions, but the final selectivity is limited by the performance and stability of the Pt/C-GDE. Therefore, future efforts to further enhance the reduction performance of the counter electrode and optimize the cell design are crucial for achieving high-efficiency flow production of benzaldehyde without bias.

Conclusions

In conclusion, we developed a $BiVO_4$/BiOCl heterostructure photoanode for the PEC conversion of toluene to benzaldehyde.

The photoanode effectively and selectively activates benzylic C(sp^3)–H bonds under both oxygen-rich and ambient conditions, achieving nearly 100% selectivity toward benzaldehyde. It also exhibits good selectivity in the oxidation of various substrates to produce aldehydes or ketones. Additionally, we constructed a PEC flow cell incorporating a scaled-up BiOCl/$BiVO_4$ photoanode and a Pt/C gas diffusion electrode (GDE), achieving a 42% toluene conversion rate with 77% benzaldehyde selectivity and demonstrated its practical potential under bias-free conditions. Mechanistic investigations revealed that enhanced charge separation efficiency and timely desorption of the product significantly contribute to the high selectivity, further supported by a proposed reaction pathway. Overall, this work presents a promising PEC strategy for the selective valorization of benzylic C(sp^3)–H bonds in feedstocks such as toluene, offering a sustainable route to high-value chemical production.

Author contributions

J. L. supervised the work. H. S. performed the experimental work and prepared the original manuscript. J. L. revised the manuscript. Q. W. and Y. Q. contributed to the experimental analysis and manuscript revision. All authors have given approval to the final version of the manuscript.

Conflicts of interest

There are no conflicts to declare.

Data availability

The data supporting this article have been included as part of the SI.

Supplementary information is available and includes preparation methods for samples, experimental procedures, and experimental data (XRD, UV-vis, SEM, TEM, XPS, LSV, EIS, Mott–Schottky, *J–t*, GC, KIE, DRIFTS, and ^{1}H NMR). See DOI: **https://doi.org/10.1039/d5sc03295d**.

Acknowledgements

We gratefully acknowledge the funding support from the National Key Research and Development Program of China (Grant No. 2020YFA0907300), the National Natural Science Foundation of China (Grant No. 22122903), and the Tianjin Distinguished Young Scholars Fund (Grant No. 20JCJQJC00260).

References

1 E. Brunard, V. Boquet, E. Van Elslande, T. Saget and P. Dauban, *J. Am. Chem. Soc.*, 2021, **143**, 6407–6412.
2 P. Xie, Y. Xie, B. Qian, H. Zhou, C. Xia and H. Huang, *J. Am. Chem. Soc.*, 2012, **134**, 9902–9905.
3 Y. Li, H. Bai, Q. Gao, K. Liu, J. Han, W. Li, C. Zhu and J. Xie, *Chem. Sci.*, 2024, **15**, 12511–12516.
4 S.-Y. Zhang, F.-M. Zhang and Y.-Q. Tu, *Chem. Soc. Rev.*, 2011, **40**, 1937.
5 C. Chen, X.-H. Xu, B. Yang and F.-L. Qing, *Org. Lett.*, 2014, **16**, 3372–3375.
6 T. G. Saint-Denis, R.-Y. Zhu, G. Chen, Q.-F. Wu and J.-Q. Yu, *Science*, 2018, **359**, eaao4798.
7 Y. Kuang, H. Cao, H. Tang, J. Chew, W. Chen, X. Shi and J. Wu, *Chem. Sci.*, 2020, **11**, 8912–8918.
8 R. Miguélez, N. Semleit, C. Rodríguez-Arias, P. Mykhailiuk, J. M. González, G. Haberhauer and P. Barrio, *Angew. Chem., Int. Ed.*, 2023, **62**, e202305296.
9 D. A. Strassfeld, C.-Y. Chen, H. S. Park, D. Q. Phan and J.-Q. Yu, *Nature*, 2023, **622**, 80–86.
10 D. Murindababisha, A. Yusuf, Y. Sun, C. Wang, Y. Ren, J. Lv, H. Xiao, G. Z. Chen and J. He, *Environ. Sci. Pollut. Res.*, 2021, **28**, 62030–62060.
11 Z. Yin, Z. Gao, L. Luo, X. Zhang, W. Hou, W. Dai, S. Tian, X. Qin, M. Wang, M. Peng, K. Li, S. Wang, L. Zhang, H. Wang, J. Li, Q. Zhu, B. Cheng, Z. Yin and D. Ma, *Angew. Chem., Int. Ed.*, 2024, e202415044.
12 H. M. Lapa and L. M. D. R. S. Martins, *ACS Omega*, 2024, **9**, 26780–26804.
13 Y. Park, K. J. McDonald and K.-S. Choi, *Chem. Soc. Rev.*, 2013, **42**, 2321–2337.
14 R. Gao, D. He, L. Wu, K. Hu, X. Liu, Y. Su and L. Wang, *Angew. Chem., Int. Ed.*, 2020, **59**, 6213–6218.
15 K. Zhang, J. Liu, L. Wang, B. Jin, X. Yang, S. Zhang and J. H. Park, *J. Am. Chem. Soc.*, 2020, **142**, 8641–8648.
16 B. Zhang, S. Yu, Y. Dai, X. Huang, L. Chou, G. Lu, G. Dong and Y. Bi, *Nat. Commun.*, 2021, **12**, 6969.
17 H. Shi, H. Guo, S. Wang, G. Zhang, Y. Hu, W. Jiang and G. Liu, *Energy Fuels*, 2022, **36**, 11404–11427.
18 J. Cheng, L. Wu and J. Luo, *Nat. Commun.*, 2023, **14**, 7228.
19 M. Xiao, Z. Wang, K. Maeda, G. Liu and L. Wang, *Chem. Sci.*, 2023, **14**, 3415–3427.
20 Z. Wang, R. R. Roberts, G. F. Naterer and K. S. Gabriel, *Int. J. Hydrogen Energy*, 2012, **37**, 16287–16301.
21 H. G. Cha and K.-S. Choi, *Nat. Chem.*, 2015, **7**, 328–333.
22 Y. Sun, L. Han and P. Strasser, *Chem. Soc. Rev.*, 2020, **49**, 6605–6631.
23 K. Obata, M. Schwarze, T. A. Thiel, X. Zhang, B. Radhakrishnan, I. Y. Ahmet, R. Van De Krol, R. Schomäcker and F. F. Abdi, *Nat. Commun.*, 2023, **14**, 6017.
24 Y. Zhong, H. Xiong, J. Low, R. Long and Y. Xiong, *eScience*, 2023, **3**, 100086.
25 A. Li, P. Zhang, E. Kan and J. Gong, *eScience*, 2024, **4**, 100157.
26 L. Zhang, L. Liardet, J. Luo, D. Ren, M. Grätzel and X. Hu, *Nat. Catal.*, 2019, **2**, 366–373.
27 J. Wang, C. Yang, H. Gao, L. Zuo, Z. Guo, P. Yang, S. Li and Z. Tang, *Angew. Chem., Int. Ed.*, 2024, **136**, e202408901.
28 A. Shi, P. Xie, Y. Wang and Y. Qiu, *Nat. Commun.*, 2025, **16**, 2322.
29 Y. Chen, Y. He, Y. Gao, J. Xue, W. Qu, J. Xuan and Y. Mo, *Science*, 2024, **384**, 670–676.
30 L. Luo, W. Chen, S.-M. Xu, J. Yang, M. Li, H. Zhou, M. Xu, M. Shao, X. Kong, Z. Li and H. Duan, *J. Am. Chem. Soc.*, 2022, **144**, 7720–7730.

31 Y. Lu, B. G. Lee, C. Lin, T.-K. Liu, Z. Wang, J. Miao, S. H. Oh, K. C. Kim, K. Zhang and J. H. Park, *Nat. Commun.*, 2024, **15**, 5475.
32 Y. Zhao, C. Deng, D. Tang, L. Ding, Y. Zhang, H. Sheng, H. Ji, W. Song, W. Ma, C. Chen and J. Zhao, *Nat. Catal.*, 2021, **4**, 684–691.
33 Y. Zhao, M. Duan, C. Deng, J. Yang, S. Yang, Y. Zhang, H. Sheng, Y. Li, C. Chen and J. Zhao, *Nat. Commun.*, 2023, **14**, 1943.
34 Q. Wang, L. Wu, H. Shi and J. Luo, *ACS Energy Lett.*, 2025, **10**, 2026–2034.
35 Y. Yang, X. Yang, L. Tang, S. Sung, Z. Wang, Z. Lu, S. H. Oh, Q. Zhong, J. H. Park and K. Zhang, *Adv. Mater.*, 2025, 2502321.
36 X. Cao, Z. Chen, R. Lin, W.-C. Cheong, S. Liu, J. Zhang, Q. Peng, C. Chen, T. Han, X. Tong, Y. Wang, R. Shen, W. Zhu, D. Wang and Y. Li, *Nat. Catal.*, 2018, **1**, 704–710.
37 H. Wang, C. Cao, D. Li, Y. Ge, R. Chen, R. Song, W. Gao, X. Wang, X. Deng, H. Zhang, B. Ye, Z. Li and C. Li, *J. Am. Chem. Soc.*, 2023, **145**, 16852–16861.
38 Z. Xue, J. Yang, L. Ma, H. Li, L. Luo, K. Ji, Z. Li, X. Kong, M. Shao, L. Zheng, M. Xu and H. Duan, *ACS Catal.*, 2024, **14**, 249–261.
39 Y. Shi, P. Li, H. Chen, Z. Wang, Y. Song, Y. Tang, S. Lin, Z. Yu, L. Wu, J. C. Yu and X. Fu, *Nat. Commun.*, 2024, **15**, 4641.
40 D. Tsukamoto, Y. Shiraishi and T. Hirai, *Catal. Sci. Technol.*, 2013, **3**, 2270.
41 L.-N. Song, F. Ding, Y.-K. Yang, D. Ding, L. Chen, C.-T. Au and S.-F. Yin, *ACS Sustainable Chem. Eng.*, 2018, **6**, 17044–17050.
42 P. Chen, F. Liu, H. Ding, S. Chen, L. Chen, Y.-J. Li, C.-T. Au and S.-F. Yin, *Appl. Catal., B*, 2019, **252**, 33–40.
43 F. Liu, C.-X. Xiao, L.-H. Meng, L. Chen, Q. Zhang, J.-B. Liu, S. Shen, J.-K. Guo, C.-T. Au and S.-F. Yin, *ACS Sustainable Chem. Eng.*, 2020, **8**, 1302–1310.
44 Y.-X. Tan, Z.-M. Chai, B.-H. Wang, S. Tian, X.-X. Deng, Z.-J. Bai, L. Chen, S. Shen, J.-K. Guo, M.-Q. Cai, C.-T. Au and S.-F. Yin, *ACS Catal.*, 2021, **11**, 2492–2503.
45 B. Seo, W. H. Lee, Y. J. Sa, U. Lee, H.-S. Oh and H. Lee, *Appl. Surf. Sci.*, 2020, **534**, 147517.
46 Y. Lv, A. Kong, H. Zhang, W. Yang, Y. Chen, M. Liu, Y. Fu, J. Zhang and W. Li, *Appl. Surf. Sci.*, 2022, **599**, 153916.
47 Y. Shen, Z. Yan and K. Wang, *Chem. Eng. J.*, 2024, **488**, 150857.
48 T. Hisatomi, J. Kubota and K. Domen, *Chem. Soc. Rev.*, 2014, **43**, 7520–7535.
49 W. Yang, R. R. Prabhakar, J. Tan, S. D. Tilley and J. Moon, *Chem. Soc. Rev.*, 2019, **48**, 4979–5015.
50 J. Yu, J. González-Cobos, F. Dappozze, P. Vernoux, A. Caravaca and C. Guillard, *Green Chem.*, 2024, **26**, 1682–1708.
51 T. W. Kim and K.-S. Choi, *Science*, 2014, **343**, 990–994.
52 F. Li, W. Zhao and D. Y. C. Leung, *Appl. Catal., B*, 2019, **258**, 117954.
53 K. Li, Y. Tang, Y. Xu, Y. Wang, Y. Huo, H. Li and J. Jia, *Appl. Catal., B*, 2013, **140–141**, 179–188.
54 C. Liu, J. Zhou, J. Su and L. Guo, *Appl. Catal., B*, 2019, **241**, 506–513.
55 E. M. Simmons and J. F. Hartwig, *Angew. Chem., Int. Ed.*, 2012, **51**, 3066–3072.
56 E. C. M. Tse, J. A. Varnell, T. T. H. Hoang and A. A. Gewirth, *J. Phys. Chem. Lett.*, 2016, **7**, 3542–3547.
57 Y. Wei, X. Q. Zuo, Z. D. He, W. Chen, C. H. Lin, J. Cai, M. Sartin and Y.-X. Chen, *Electrochem. Commun.*, 2017, **81**, 1–4.
58 Y. Li, H. Zhang and Q. Liu, *Spectrochim. Acta*, 2012, **86**, 51–55.
59 X. Yang, Z. Fan, Z. Shen and M. Li, *Electrochim. Acta*, 2017, **226**, 53–59.
60 A. Lu, H. Sun, N. Zhang, L. Che, S. Shan, J. Luo, J. Zheng, L. Yang, D.-L. Peng, C.-J. Zhong and B. Chen, *ACS Catal.*, 2019, **9**, 7431–7442.
61 S. Mo, Q. Zhang, J. Li, Y. Sun, Q. Ren, S. Zou, Q. Zhang, J. Lu, M. Fu, D. Mo, J. Wu, H. Huang and D. Ye, *Appl. Catal., B*, 2020, **264**, 118464.
62 F. Kang, Q. Wang, D. Du, L. Wu, D. W. F. Cheung and J. Luo, *Angew. Chem., Int. Ed.*, 2024, **64**, e202417648.
63 R. C. Dunbar, *J. Am. Chem. Soc.*, 1973, **95**, 472–476.
64 J. C. Choe, *J. Phys. Chem. A*, 2006, **110**, 7655–7662.